Dipolar interactions in arrays of ferromagnetic nanowires: a micromagnetic study

Fatih Zighem, Thomas Maurer, Frédéric Ott and Grégory Chaboussant
Laboratoire Léon Brillouin, IRAMIS, CEA-CNRS UMR 12, CE-Saclay, 91191 Gif sur Yvette, France

We explore the behavior of periodic arrays of magnetic nanowires by micromagnetic simulations using the Nmag modeling package. A large number of modeling studies on such arrays of nanowires have been performed using finite size models. We show that these finite size micromagnetic descriptions can only be used in specific situations. We perform a systematic study of more or less dense 1D and 2D arrays of nanowires using either finite size or infinite size models and we show that finite size models fail to capture some of the features of real infinite systems. We show that the mean field model scaled to the system porosity is valid. This work can be used as a basis to the extension of micromagnetic calculations of the magnetization dynamics in arrays of nanowires.

PACS numbers: 62.23.Hj, 75.75.-c; 75.78.Cd; 75.60.Jk; 75.60.-d;
Keywords: magnetic nanowires, computational micromagnetism, magnetization curves, dipolar interactions

I. INTRODUCTION

During the past decade, fast progress has been made in the synthesis of nano-objects. In particular, efforts have been made in the synthesis of magnetic nanowires. Several routes have been developed for the preparation of such objects. The most studied consists in the electrochemical deposition using porous polycarbonate or anodic alumina (Al_2O_3) membranes as templates [1–9]. The static magnetic properties have been intensively studied by magnetometry experiments [1–9] while the dynamic magnetic properties have been probed by Ferromagnetic Resonance (FMR) [10–13] and Brillouin Light Scattering (BLS) [14–16] experiments. Among the various issues at stake for a comprehensive understanding of these materials is the influence of long-range dipolar interactions between nanowires. In fact, as shown in previous studies, the dipolar coupling between neighboring wires can considerably reduce the coercive field of an assembly of wires [17, 18]. In addition, the magnetic moments distribution inside a wire can be strongly affected by stray fields originating from neighboring wires, and the usual coherent rotation approximation is then not justified [19]. Another manifestation of dipolar interactions concerns the magnetic excitations (spin waves) which were shown to be strongly dependent on the demagnetizing field and on surfaces and interfaces boundaries [14, 20]. A rigorous analysis of the static and dynamic measurements requires then to take into account these dipolar interactions. In some cases, dipolar interactions are taken into account by considering nanowires as dipoles [17, 21] but this approximation is only justified when the distribution of magnetic moments inside the nanowire is uniform, allowing for an analytical treatment of the magnetic interaction between neighboring wires[22].

The scope of this study is to quantify the dipolar interactions in various geometries of nanowires arrays (see Figure 1). Our micromagnetic calculations take explicitly into account the dipolar interactions between nanowires, and we focus on the static magnetic properties via the calculation of magnetization curves measured in different directions between the nanowire's axis and the applied magnetic field direction. The paper is structured as follows: the magnetic parameters of the studied systems are presented in section II. Section III and IV are devoted to the study of the magnetostatic interactions in linear rows of nanowires and in hexagonal arrays of nanowires, respectively.

II. MAGNETIC PARAMETERS AND GEOMETRY OF THE NANOWIRES

Throughout this communication, the basic building brick which is considered is a Co magnetic nanowire of length (ℓ) 100 nm and diameter (d) 10 nm. These dimensions are typical of real materials [16, 23, 24]. The diameter of the wire has been chosen so that a coherent rotation is expected. The diameter for coherent magnetic rotation in Co spheres is 15 nm. The length of the wire has been chosen to be 10 times the diameter so that the shape anisotropy is very close to that of an infinite cylinder. The demagnetizing coefficient for an ellipsoid with an aspect ratio of 10 is 0.017 which is very close to 0. The limitation to a length of 100 nm allows to perform more complex micromagnetic simulations than would be possible with longer wires while keeping the key property of a strong shape anisotropy.

The magnetic parameters used correspond to typical value for hcp cobalt thin films [25]: magnetization saturation $M_S = 1.4 \times 10^6$ A.m^{-1}, exchange stiffness $A = 1.2 \times 10^{-11}$ J.m^{-1}, the magnetocrystalline anisotropy is neglected. The exchange length, defined as $\ell_{ex} = \sqrt{2A/\mu_0 M_S^2}$, is around 3.2 nm. We have used the Nmag micromagnetic modelling package [26], which is a finite element code, in order to solve the Landau-Lifshtiz-Gilbert equation. In our simulations, the damping (Gilbert) constant α was set to 0.5 in order to minimize the computing time and because we are only interested in the static magnetization configurations [26]. The nanowires were meshed with Netgen [27] so

that the distance between two nodes is of the order of 2 nm, being smaller than the exchange length (ℓ_{ex}). We have checked that the results obtained with a finer mesh (1 nm between two nodes) are identical. Our convention is that the wires axis is Ox direction (see Figure 1a). The magnetization reversal of the different systems has been studied through magnetization curves calculations along the three directions (Ox, Oy and Oz). The magnetization curves are investigated by applying external magnetic fields B ranging from -1800 mT to $+1800$ mT and back to -1800 mT, the field is incremented in steps of 12 mT. Note that m_i corresponds to the projected reduced magnetization (M_i/M_S) along i (x, y or z).

For a field applied along the wire axis in the case of an isolated nanowire, a square hysteresis loop is obtained which indicates that the nanowire switches between two homogeneously magnetized states [28, 29]. The coercive field $\mu_0 H_C \simeq 470$ mT to be compared with $\mu_0 H_C \simeq 827$ mT in the case of an ellipsoid with the same aspect ratio [30]. For a field applied perpendicular to the wire axis (along Oy or Oz: hard axis directions), the saturation field is $\mu_0 H_S \simeq 800$ mT which is very close to that of an ellipsoid with the same aspect ratio $\mu_0 H_S \simeq 827$ mT (see supplementary Figure S1) .

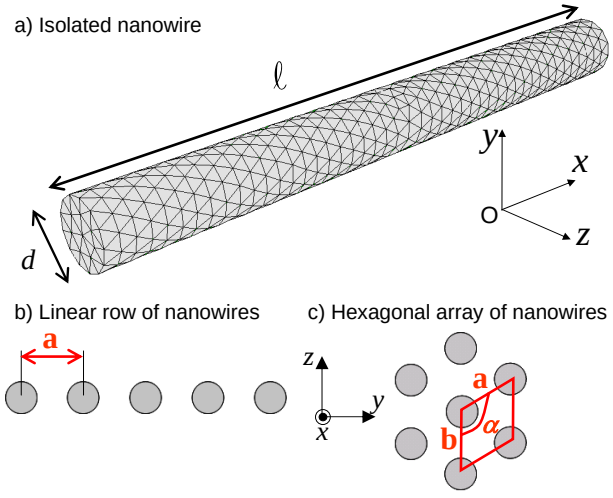

Figure 1: a) Typical mesh used for the micromagnetic calculations ($\ell = 100$ nm and $d = 10$ nm). The mesh is composed of 700 nodes and the distance between two nodes is around 2 nm. The wire axis is along the Ox direction. b) Top view ((yOz) plane) of a linear row of 5 nanowires along Oy. c) Top view of an hexagonal array of 7 nanowires ($a = b$ and $\alpha = 120°$) .

III. LINEAR ROWS OF NANOWIRES

A. Finite rows

In order to address the influence of dipolar interactions, we have first examined the case of a finite number of nanowires ($N = 3$ to 13), ordered parallel to each other along the Oy direction (see Figure 1b). The distance between the wires centers (a) was varied from 15 to 60 nm, that is from $1.5d$ to $6d$. For an inter-wire distance larger than 50 nm, we did not find any significant difference in the magnetization curves from the simple case of an isolated nanowire.

The stable remanent states in these row arrangements depend on both the amplitude and direction of the magnetic field initially applied. The remanent state obtained after applying a saturating field along Ox corresponds to an alignment of all the magnetic moments along Ox even for small a-values. On the other hand, the remanent state after applying a saturating field along Oy or Oz depends on both the distance a and the number of interacting nanowires. The general behavior is that the magnetic moments inside the nanowires are quasi-homogeneously magnetized and only the total magnetization direction ($+Ox$ or $-Ox$) changes from a nanowire to the next. However, the system does not necessarily adopt a perfect "antiferromagnetic" ($\cdots$up-down-up-down$\cdots$) configuration.

Figure 2a presents typical magnetization curves obtained for a 7 nanowires row as a function of the inter-wire distance and a field applied along Ox. The magnetization curves present plateaus which correspond to the switching of a single wire of the row. This was experimentally put into evidence in magnetic microwires by Sampaio et al . [18]. However, in our simulations we observe that the widths of the plateaus tend to increase when a decreases and that the last plateaus (next to the last and last wire to switch) are more extended than the first plateaus (see Figure 2a). This is qualitatively different from the behavior experimentally observed in [18]. We attribute this to the fact that in the experimental measurements, $d \ll a$ so that dipolar effects were limited. On the other hand, in our calculations, $d \sim a$, so that dipolar effects play a key role: the energy barrier for the last wire switch is thus greatly enhanced because of dipolar fields from the other wires which opposes the last wire switch. .

Figure 2b presents the switching field of the central nanowire for different types of rows. In all cases, the central nanowire switches first due to a maximum intensity of the dipolar field created by the surrounding nanowires. Figure2 illustrates 2 points: (i) there is an inter-wire distance ($a > 60$ nm) for which the dipolar coupling can be neglected. (ii) when dipolar coupling between wires is significant ($a < 60$ nm), it is nevertheless only necessary to take into account a rather small number of neighbours

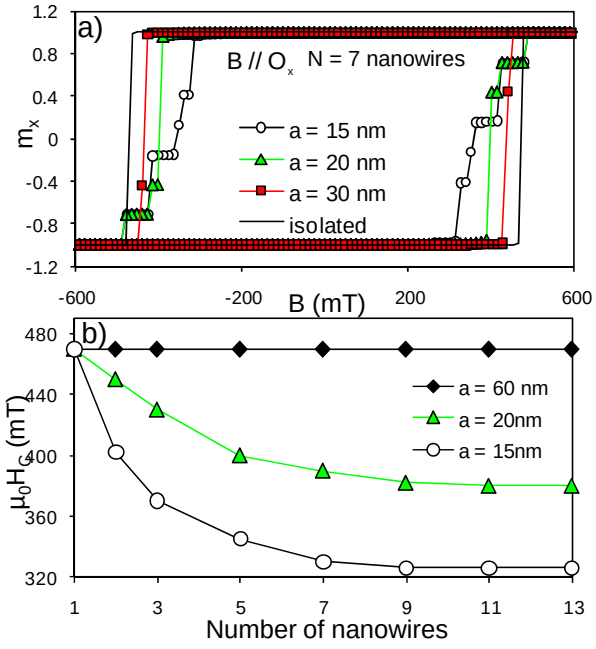

Figure 2: a) Magnetization curves calculated with $B \parallel Ox$ for different inter-wire distances in a row formed by $N = 7$ nanowires. The solid black line corresponds to the hysteresis cycle of an isolated nanowire. b) Evolution of the coercive field of the central nanowire as a function of the number of nanowires. Calculated values for three different inter-wire distances ($a = 15, 20, 60$ nm) are shown. Lines are guided for the eyes.

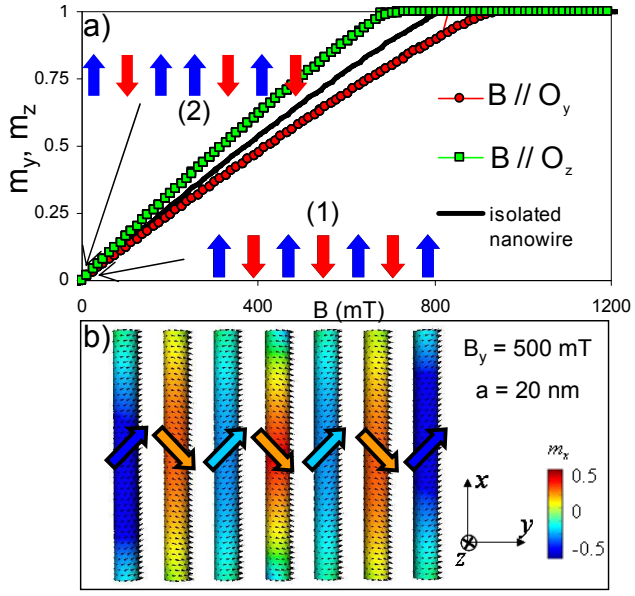

Figure 3: a) Magnetization curves calculated along y (triangles) and z (circles) for a row of $N = 7$ nanowires ($a = 20$ nm). The solid line is the magnetization curve along the hard axis of an isolated nanowire. We have also represented a sketch of the remanent state obtained after applying B along Oy (1) and along Oz (2). b) Magnetic moments distribution when the system is subjected to a transverse (along Oy) magnetic field of 500 mT.

(3 on each side) to converge towards the infinite case. This shows that demagnetizing field effects are small in the case of 1D chains.

Figure 3a presents the magnetization curves for a field $\vec{B}$ applied along Oy and Oz on a row of $N = 7$ nanowires. The saturation along Oz is reached for an applied field larger than along Oy. Indeed, when the nanowires are close (i. e. $a \to 10$ nm) and for a large number of nanowires, the system can be viewed as an infinite strip along Oy, which defines a second easy axis (in addition to the one along Ox defined by the shape anisotropy of the nanowires). In these conditions, the Oz direction can be defined as a hard axis and a larger applied field will be necessary to reach the magnetization saturation in this direction (see Figure 4a for an infinite row of nanowires). The dipolar field created by a given wire strongly depends on the magnetic moments distribution inside the wire; thus, when the magnetic moments begin to orient along the Oz direction (with $B \parallel Oz$), the stray fields created on its neighbors will point in the $-Oz$ direction (in first approximation) and will not favor alignment along Oz. On the contrary, when the magnetic moments begin to orient along the Oy direction (with $B \parallel Oy$), the stray fields created on its neighbors favor an alignment along Oy (see Figure 3b). Note that, as illustrated in Figure 3b, non uniform magnetic moments distributions appear inside the wires under applied magnetic field. This effect could be a source of localized spin waves modes, as proposed in Ref. [31].

B. Infinite rows

We have used the hybrid "finite element/boundary element" method [32] available in the Nmag package to model an infinite row of nanowires. A particular importance is given to the choice of the elementary meshed cell as the results can strongly depend on it. The elementary cell is composed of 10 wires in order to have a large cell and a reasonable computing time. In this method, to take into account the long-range dipolar interaction between the nanowires, virtual copies of the elementary cell are created [26, 32]. 40 virtual copies (20 to the left and 20 to the right of the meshed cell) have been used in the following simulations.

When $B \parallel Ox$, the zero field configuration corresponds to a parallel alignment of the magnetic moments along Ox. The wires are subjected to the same dipolar field created by the neighboring wires and switch all for the same applied field. The net result is a reinforcement and an homogeneization of the demagnetizing field which explains why the magnetization is reversed for a smaller applied field compared to the isolated wire situation. The coercive fields $\mu_0 H_C$ in infinite rows (see Figure 4a)

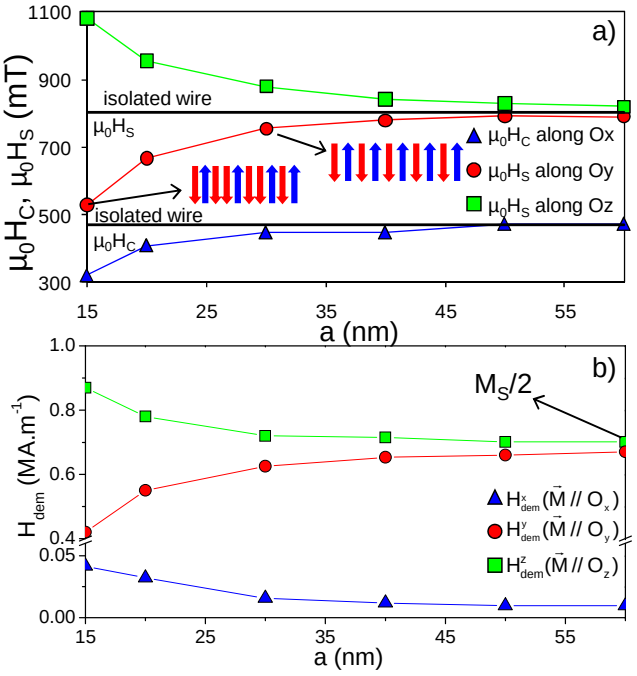

Figure 4: a) Coercive (triangles) and saturation (circles and squares) fields obtained from calculated magnetization curves along Ox, Oy and Oz direction, respectively. Sketches represent zero field configurations after applying a saturating field along y. Lines are guided for the eyes. b) x- (triangles), y- (circles) and z- (squares) components of the demagnetizing field calculated in an infinite row respectively saturated along Ox, Oy and Oz as a function of the inter-wire distance a.

are then very close to the ones obtained for the central nanowire of rows composed by 9 or more nanowires (see Figure 2b).

When $B \parallel Oy$ or Oz, the zero field state corresponds to magnetized wires randomly aligned along $+Ox$ or $-Ox$ and we find that it strongly depends not only on the distance a but also in the choice of the elementary cell. Figure 4a presents the saturation fields $\mu_0 H_S$ obtained from the magnetization curves calculated along Oy and Oz. We found that $\mu_0 H_S$ (measured along Oy or Oz) is not affected if a larger elementary cell is chosen despite the fact that different remanent state are obtained. This indicates that defects in the perfect "antiferromagnetic" remanent state ($\cdots$up-down-up-down$\cdots$) have pratically no influence in the magnetization reversal. Finally, as expected, for a larger than 50 nm, the dipolar interactions are negligible and the macroscopic ($\mu_0 H_S$ and $\mu_0 H_C$) values measured are close to the ones obtained for isolated wires.

In addition, we have represents (see Figure 4b) the x-, y- and z-components of the demagnetizing field calculated in the infinite row respectively saturated along Ox, Oy and Oz as a function of the inter-wire distance a. As explained previoulsy, when $a \to 10$ nm, the system can be viewed as an infinite stripe along Oy. This is confirmed by the y- (resp. z-) component of the demagnetizing field which strongly decreases (resp. increases) when a decreases and explained why a smaller (resp. larger) field is necessary to saturate the system along Oy (resp. Oz) (see Figure 4a). Moreover, the x-component of the demagnetizing slowly decreases with a; it confirms that the easy axis along the Ox direction is less pronounced for small inter-wire distance.

To summarize, these results show that some aspects of the static magnetic properties of an infinite row of nanowires could be analyzed by using a finite but sufficiently large number of interacting nanowires.

IV. HEXAGONAL ARRAYS OF NANOWIRES

In this section, we consider hexagonal arrays of Co nanowires. The choice of this arrangement is motivated by the fact that synthesis routes, such as electrodeposition, lead to the fabrication of well defined hexagonal arrays of nanowires with excellent control of their diameter (d), length (ℓ) and inter-wire distance (a) [23, 24]. For large inter-wire distances, the magnetic properties of these systems are easily analyzed as one can neglect the dipolar couplings between the nanowires. For small inter-wire distances (dense array of nanowires), the dipolar coupling between the nanowires must be taken into account in the static and dynamic magnetic properties. Until now, the magnetic behavior of such systems are generally analyzed by using a finite number of interacting nanowires [33, 34] or by a phenomenological treatment of the dipolar coupling [35–37]. We propose here to compare finite and infinite hexagonal arrays of nanowires.

A. Finite size arrays

Three different arrays are considered. They are defined by the number of interacting nanowires: 7 (see Figure 1c), 16 (4×4) and 30 (6×5). The inter-wire distance (a) is varied from 15 to 40 nm, that is from $1.5d$ to $4d$. The length (ℓ) and diameter (d) of the nanowires are 100 and 10 nm, respectively.

The remanent state derived from magnetization curves calculated along Ox (see Figures 6a) corresponds to an alignment of the magnetic moments along x. The magnetization reversal takes place in several steps (see Figure 5a-b) defined by the magnetization switching of one or more nanowires between $+Ox$ to $-Ox$. These steps are clearly revealed by several magnetization plateaux in the hysteresis cycles. Just before an individual nanowire switches, the y- and z-components of the magnetic

moments located at the tips significantly increase and act as nucleation points for the magnetization reversal process. Moreover, when the nanowires have almost completely switched, a plateau of several mT can appear in the hysteresis cycle (a = 15 nm and $B < -400$ mT in Figure 5b). This plateau is due to the finite size of the system: the dipolar field created by the switched nanowires hinders the switch of the last nanowires.

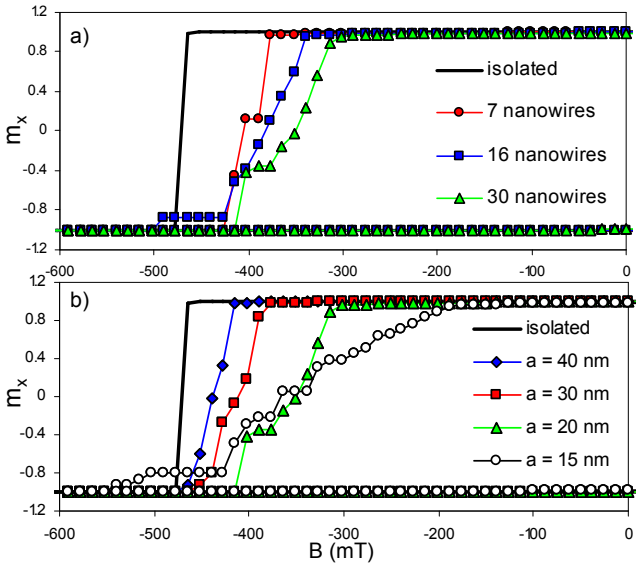

Figure 5: a) Hysteresis curves for a field applied along Ox on hexagonal arrays of different sizes with a = 20 nm. b) Hysteresis cycles calculated for an array of 30 nanowires for different inter-wire distances. The solid black line is the cycle obtained for an isolated nanowire.

Figure 6a shows a top view of the magnetic moments distribution obtained for an array of 30 nanowires as a function of B_x. These micromagnetic configurations have been extracted from the hysteresis cycle (with a = 20 nm). It can be observed that just before the magnetization reversal ($B_x = -302$ mT), m_x is close to zero at the tips (see Figure 6b). Moreover, the reversal of the system behaves similar to the domain wall propagation in thin films rather than a random switching of the wires. When increasing the number of interacting nanowires (see Figure 5a) or reducing the period of the array (see Figure 5b), the hysteresis cycles are less square due to the dipolar coupling between the objects; the coercive field is then reduced by 25% for 30 nanowires (with a = 20 nm) compared to the coercive field obtained for isolated nanowires.

The remanent state presented just above (quasi-homogeneously magnetized nanowires) is not the only stable state. Other remanent micromagnetic configurations appear when applying a saturating magnetic field along Oy or Oz (see Figure 7). They correspond to a random orientation $+Ox$ or $-Ox$ of the nanowire's

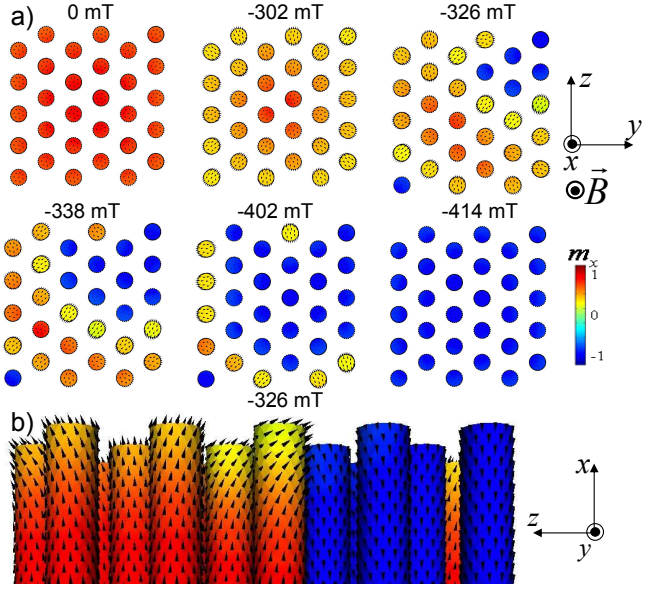

Figure 6: Array of 30 interacting nanowires (a = 20 nm): a) top view of the magnetic moments distribution as a function of B_x. At zero applied field, the magnetization is quasi-homogeneous and aligned along Ox; when increasing B_x, the nanowires switch one after the other and the system is saturated along $-Ox$ for an applied field larger than -415 mT. Colors encode m_x. b) Side view of the system ($B_x = -326$ mT) showing the increased of the m_y and m_z components before the magnetization reversal.

magnetizations, apart for the case ($a = 20$ nm; $B \parallel Oy$), where an antiferromagnetic order appears. These remanent states are more stable than the one presented in Figure 8 because they minimize the demagnetizing field inside the nanowires more efficiently. Figure 7c shows the total energy E_{tot} (kJ.m^{-3}) of the different remanent states. It shows that the states obtained after applying a saturating field along Oy or Oz have a lower total energy than the one obtained in absence of dipolar coupling. E_{tot} is large when all the nanowires are fully magnetized in the same direction ($B_{sat} \parallel Ox$) and diminishes when a increases (i. e. when the dipolar coupling weakens). For random wire orientation ($B_{sat} \parallel Oy$ or $B_{sat} \parallel Oz$), the magnetic energy decreases when a decreases. This is due to the fact that flux closure is more efficient for the random orientation of the nanowires.

The magnetization curves calculated along Oy and Oz are identical contrary to the row case (Section III). The applied field necessary to ensure magnetization saturation along y or z is around 750 mT (for a in the range {15-40 nm}), and it depends weakly on the number of interacting nanowires N (in the range $\{7-30\}$). Moreover, inside a nanowire, the magnetization reversal is almost coherent contrary to the magnetization curves calculated along Ox where we find non uniform distributions of the magnetic moments at the tips which act as nucleation points for the magnetization reversal.

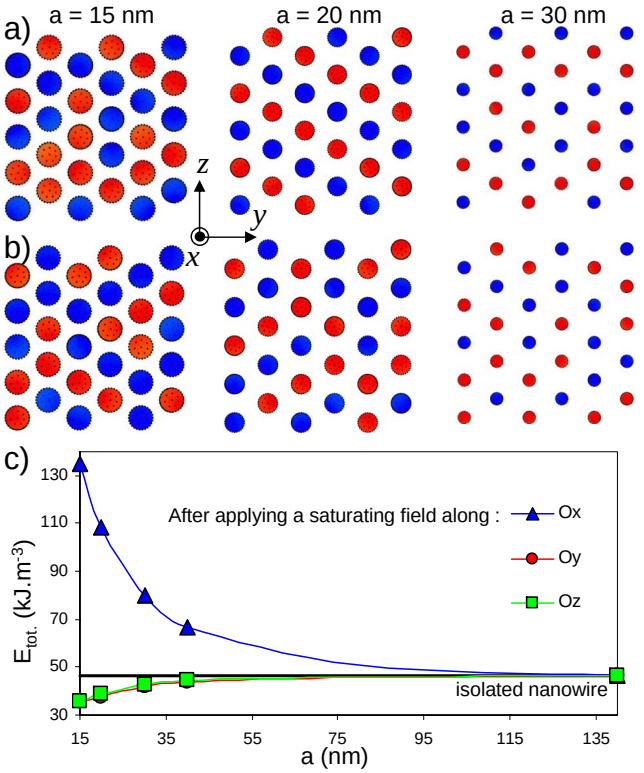

Figure 7: Array of 30 interacting nanowires. a) and b) Remanent states after applying a saturating field along Oy (a) and Oz (b) for different inter-wire distances. b) Total energy at remanence after applying a magnetic field along x, y and z as function of the inter-wire distance.

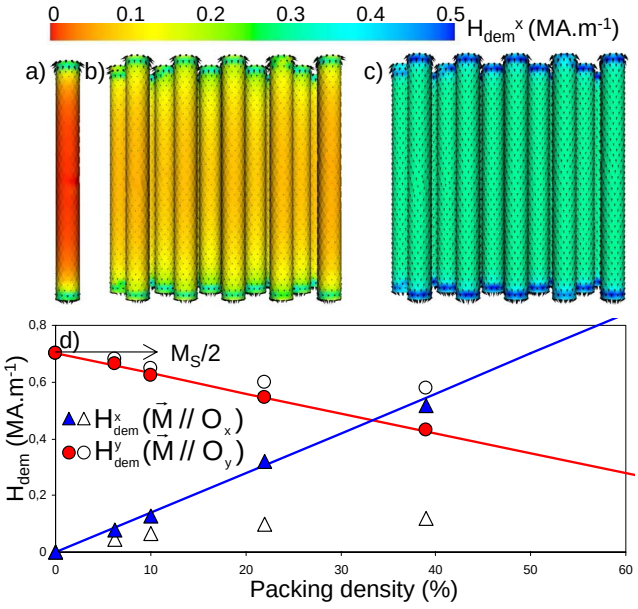

Figure 8: a-b-c) Side view of the demagnetizing field distribution acting inside the nanowire at remanence (after applying a saturating field along Ox) for: a) an isolated nanowire, b) a finite array of 30 nanowires with $a = 20$ nm and c) an infinite array of nanowires (elementary cell: 30 nanowires with $a = 20$ nm). The colors encode the x-component of the demagnetizing field $-H^x_{dem.}\cdot$ ($\times 10^6$A.m^{-1}). d) x- (filled triangles) and y- (filled circles) components of the demagnetizing field measured in an infinite array of nanowires homogeneously magnetized respectively along Ox and Oy as a function of the packing density P. The solid lines correspond to the mean field modelization [36, 37]. Unfilled symbols correspond to the values obtained in finite size arrays of 30 interacting nanowires.

B. Infinite periodic arrays

The chosen elementary cell corresponds to an array of 30 nanowires. We have considered a finite number of 20×20 virtual copies (12000 interacting nanowires) of the elementary cell [32] for the calculation of the dipolar coupling between the nanowires. The periodic boundary conditions have been applied for different inter-wire distances: $a = 15$, 20, 30 and 40 nm. We have thus perform micromagnetic simulations for hexagonal arrays of nanowires with a packing density P in the range $\{0\% - 40\%\}$. In the case $a = 15$ nm ($P \sim 40\%$), the periodic boundary conditions can-not be applied properly since the separation between the nanowires is smaller than $2d$ along the Oz direction. However, simulations can nevertheless be done by considering small defects in the geometrical arrangement along the Oz direction (see supplementary Figure S2).

For an applied magnetic field $B \parallel Ox$, for $a \geqslant 20$ nm, the remanent states consist of wires magnetized in the same direction along Ox which is similar to what was obtained in the case of finite arrays (Figure 5b and 6a) where the remanence was 1. However, in the case $a = 15$ nm, a fraction of wires ($\sim 15\%$) have switched, so that the remanence is only 0.7. This is due to the fact that for large packing densities, the demagnetizing fields start to play a significant role and are able to overcome the wires shape anisotropy. This aspect is completely overlooked in finite size array simulations. This is illustrated on Figure 9 where the hysteresis cycles in the case of finite size and infinite size arrays calculations are compared. Very large differences can be observed in the shapes of the hysteresis curves. Figure 8 presents the demagnetizing field distributions inside an isolated nanowire, a finite array of 30 nanowires ($a = 20$ nm) and an infinite array of nanowires (elementary cell of 30 nanowires with $a = 20$ nm). For an isolated nanowire, the demagnetizing field $\vec{H}_{dem}$ is localized at the tips of the nanowire and is close to zero in the central part of the nanowire [28, 29]. When 30 nanowires interact, $\vec{H}_{dem}$ is reinforced inside the nanowires ($\sim 0.1 \times 10^6$ A.m^{-1}) and takes a value of about 0.3×10^6 A.m^{-1} when an infinite array is considered. Thus, as we shall see, the magnetization reversal will be modified by the packing density P. These calculated values of the demagnetizing field can be compared to the mean field model [36, 37]. Indeed, in a simple model, when all the nanowires are

uniformly magnetized along Ox, two limiting cases can be considered as a function of P: i) $P = 0\%$ corresponds to the case of an isolated nanowire where we find that the x-component of the demagnetizing field is close to zero, ii) $P = 100\%$ corresponds to the continuous film limit where x-component of the demagnetizing field is equal to M_S. Our numerical results follow well this model (see Figure 9) and validate our numerical calculations of the dipolar interactions. Note that the mean field model can be applied only in the case of homogeneously magnetized systems whereas our simulations can take into account the dipolar coupling in the case of non uniform distributions of the magnetic moments inside the nanowires.

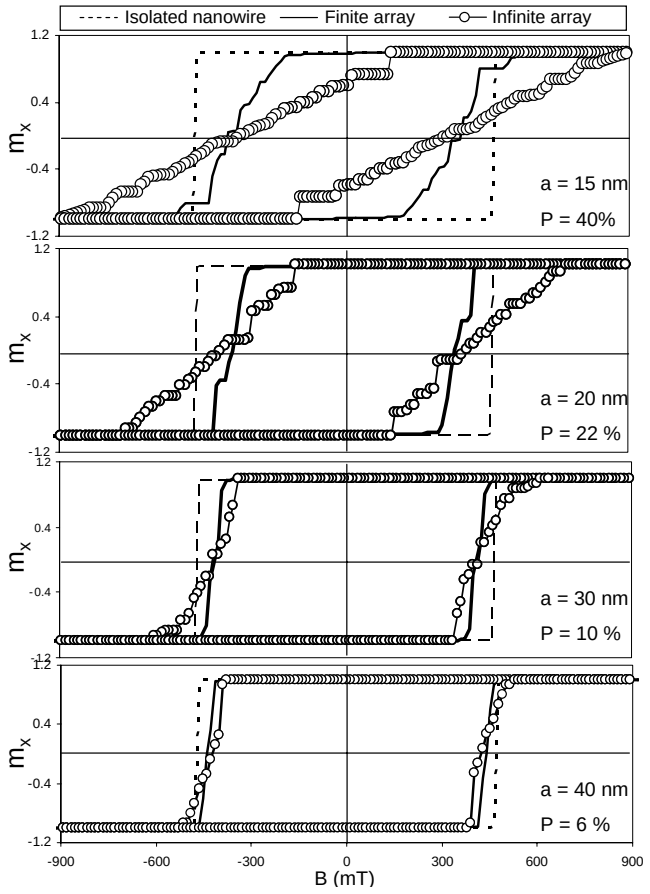

Figure 9: $B \parallel Ox$: Hysteresis curves obtained from finite (30 nanowires: solid line) and infinite (elementary cell of 30 nanowires: circles) hexagonal arrays with different inter-wire distances ($a = 15$, 20, 30, 40 nm). In each panel, the dashed lines represent the hysteresis cycle for an isolated nanowire.

On the other hand, the magnetization curves calculated along Ox (Figure 10) show strong changes, especially for large P ($a \leq 20$ nm) compared to the curves calculated with 30 interacting nanowires (Figure 5). From Figure 10, we can show that, when decreasing the inter-wire distance, the hysteresis curve calculated along Ox is less square and the saturation of the system (all magnetic moments aligned along Ox or $-Ox$) is reached for a larger applied field [35]. Moreover, the remanent magnetization is reduced to 0.7 in the case of large P. For the larger inter-wire distance ($a = 40$ nm), the hysteresis cycles do not strongly differs from the one obtained in the finite array case but, when approaching the saturation, the cycle departs from a square one. Figure 11 presents a top view of the magnetic moments distribution during the magnetization reversal. These micromagnetic configurations have been extracted from the curves calculated with $P = 22\%$. We show that the nanowires switch more randomly compared to the case of finite arrays (see Figure 6).

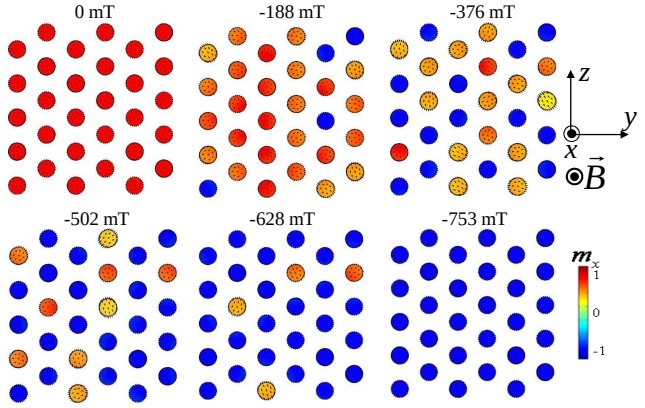

Figure 10: Periodic array of nanowires (elementary cell = 30 nanowires; $a = 20$ nm): top view of the magnetic moments distribution as a function of B_x. Colors encode m_x.

For $B \parallel Oy$ (or equivalently $B \parallel Oz$), the remanent states do not differ from the ones obtained in finite arrays of 30 interacting nanowires: they correspond to a random orientations $+Ox$ or $-Ox$ of the nanowire magnetization. Moreover, the magnetization reversal is similar to that observed in finite hexagonal array of 30 interacting nanowires, and a smaller $\mu_0 H_S$ is necessary to saturate the system as the inter-wire distance decreases (see Figure 12). The fact that magnetization curves calculated along Oy (resp. along Ox) tend to have smaller $\mu_0 H_S$ (resp. $\mu_0 H_C$) when $a \to 10$ nm or $P \to 100\%$ (i. e. that the hard (resp. easy) axis is less pronounced) is due to the continuous film limit ($P = 100\%$). In this limit (and in absence of magnetocrystalline anisotropy), the Ox direction is a hard axis whereas (yOz) becomes an easy-plane for the magnetization [23]. In addition, note that when the system is saturated along Oy (or Oz), the value of the y-component of the demagnetizing field is well fitted by using the mean field model [36, 37] as presented in Figure 9: we find that $H^y_{dem} = M_S/2$ for $P = 0\%$ (isolated nanowire) and $H^y_{dem.}$ linearly decreases and tends to zero when P increases (continuous film limit). Moreover, we find that a crossing occurs around $P \sim 1/3$ between the demagnetizing field calculated along O_x and O_y. A similar behaviour is observed in the mean

field model [36, 37] and it corresponds to the switching of the easy axis from the O_x direction to the plane (yOz).

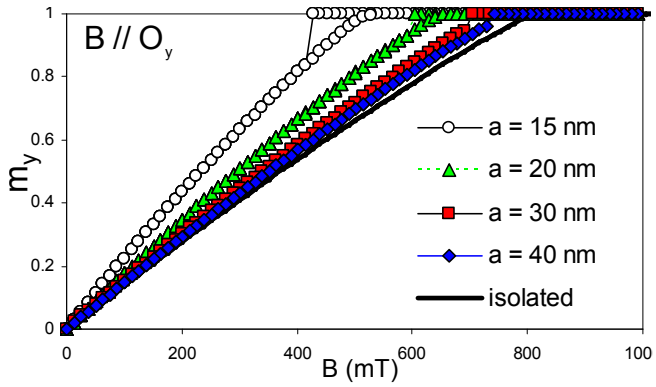

Figure 11: $B \parallel Oy$ (or equivalently $B \parallel Oz$): magnetization curves obtained from periodic (infinite) arrays with different inter-wire distances ($a = 15$, 20, 30, 40 nm).

These results show that infinite and dense hexagonal arrays of nanowires need rigorous modelizations to take into account the dipolar coupling whereas infinite arrays with larger inter-wire distance can be analyzed by using a sufficiently large but finite number of interacting nanowires.

V. CONCLUSION

We have shown that user friendly tools such as the micromagnetic package Nmag allow to perform calculation on complex extended systems. The systematic study of more or less dense systems has demonstrated the need to properly take into account the dipolar field. The use of finite size models which do not properly include dipolar fields effects fail to quantitatively reproduce the magnetic behavior of dense arrays of nanowires with packing densities larger that $P \sim 10\%$. We also show that even for wires whose size is well below the radius of coherent rotation, complex non homogeneous magnetic configurations develop in the wires under applied magnetic field. These effects are overlooked by effective field models but play a key role in the magnetic dynamics properties of these wires. A natural extension of this work will be to study the dynamics of the magnetization of these arrays and quantify the effects of the non homogeneous magnetization and demagnetizing field distributions inside the wires.

Acknowledgments

The authors gratefully acknowledge the Agence Nationale de la Recherche (ANR) for their financial support (project 07-NANO-009 MAGAFIL). We thank the NMAG developers for their advices.

[1] D. J. Sellmyer, M. Zheng and R. Skomski, J. Phys.: Condens. Matter **13**, R433 (2001)
[2] S. J. Hurst, E. K. Payne, L. Qin and C. A. Mirkin, Angew. Chem. Int. Ed. **45**, 2672 (2006)
[3] T. M. Whitney, P. C. Searson, J. S. Jiang, and C. L. Chien, Science **261** 1316 (1993)
[4] H. Pan, B. Liu, J. Yi, C. Poh, S. Lim, J. Ding, Y. Feng, C. H. A. Huan and J. Lin, J. Phys. Chem. B **109**, 3094 (2005)
[5] J. Meier, B. Doudin and J.-Ph. Ansermet, J. Appl. Phys. **79**, 6010 (1996)
[6] H. Zeng, R. Skomski, L. Menon, Y. Liu, S. Bandyopadhyay and D. J. Sellmyer, Phys. Rev. B **65**, 134426 (2002)
[7] G. C. Han, B. Y. Zong, P. Luo, and Y. H. Wu, J. Appl. Phys. **93**, 9202 (2003)
[8] X. Y. Zhang, G. H. Wen, Y. F. Chan, R. K. Zheng, X. X. Zhang, and N. Wang, Appl. Phys. Lett. **83**, 3341 (2003)
[9] M. Vazquez, M. Hernandez-Velez, K. Pirota, A. Asenjo, D. Navas, J. Velazquez, P. Vargas and C. Ramos, Eur. Phys. J. B **40**, 489 (2004)
[10] M. Demand, A. Encinas-Oropesa, S. Kenane, U. Ebels, I. Huynen and L. Piraux, J. Magn. Magn. Mater. **249**, 228 (2002)
[11] A. Sklyuyev, M. Ciureanu, C. Akyel, P. Ciureanu, and A. Yelon, J. Appl. Phys. **105**, 023914 (2009)
[12] G. Kartopu, O. Yalcin, S. Kazan, B. Aktas, J. Magn. Magn. Mater. **321**, 1142 (2009)
[13] J. De La Torre Medina, M. Darques, L. Piraux and A. Encinas, J. Appl. Phys. **105**, 023909 (2009)
[14] T. M. Nguyen, M. G. Cottam, H. Y. Liu, Z. K. Wang, S. C. Ng, M. H. Kuok, D. J. Lockwood, K. Nielsch and U. Gösele, Phys. Rev B, **73**, 140402R (2006)
[15] Z. K. Wang, H. S. Lim, V. L. Zhang, J. L. Goh, S. C. Ng, M. H. Kuok, H. L. Su and S. L. Tang, Nano Lett., 2006, **6**, 1083 (2006)
[16] A. A. Stashkevich, Y. Roussigné, P. Djemia, S. M. Chérif, P. R. Evans, A. P. Murphy, W. R. Hendren, R. Atkinson, R. J. Pollard, A. V. Zayats, G. Chaboussant and F. Ott, Phys. Rev B, **80**, 144406 (2009)
[17] J. Velazquez, C. Garcia, M. Vazquez and A. Hernando, J. Appl. Phys. **85**, 2768 (1999)
[18] L. Sampaio, E. H. C. P. Sinnecker, G. R. C. Cernicchiaro,

M. Knobel, M. Vazquez and J. Velazquez, Phys. Rev. B **61**, 8976 (2000)
[19] Y. Jaccard, Ph. Guittienne, D. Kelly, J.-E. Wegrowe and J.-Ph. Ansermet, Phys. Rev. B **62**, 1141 (2000)
[20] F. Zighem, Y. Roussigné, S. M. Chérif and P. Moch, J. Phys.: Condens. Matter **19** 176220 (2007)
[21] R. Piccin, D. Laroze, M. Knobel, P. Vargas and M. Vazquez, Eur. Phys. Letters, **78**, 67004 (2007)
[22] L. Clime, P. Ciureanu and A. Yelon, J. Magn. Magn. Mater. **297**, 60 (2006)
[23] T. Thurn-Albrecht, J. Schotter, G. A. Kästle, N. Emley, T. Shibauchi, L. Krusin-Elbaum, K. Guarini, C. T. Black, M. T. Tuominen, T. P. Russell, Science, **290,** 2216 (2000)
[24] F. Vidal, Y. Zheng, J. Milano, D. Demaille, P. Schio, E. Fonda and B. Vodungbo, Appl. Phys. Lett., **95**, 152510 (2009)
[25] P. E. Tannenwald and R. Weber, Phys. Rev. , **121**, 715 (1961)
[26] T. Fischbacher, M. Franchin, G. Bordignon and H. Fangohr, IEEE Trans. Mag. **43**, 2896 (2007), URL : http://nmag.soton.ac.uk/nmag/
[27] NETGEN, URL: http://www.hpfem.jku.at/netgen/
[28] F. Ott, T. Maurer, G. Chaboussant, Y. Soumare, J.-Y. Piquemal and G. Viau, J. Appl. Phys. **105**, 013915 (2009)
[29] T. Maurer, F. Zighem, F. Ott, G. Chaboussant, G. André, Y. Soumare, J.-Y. Piquemal, G. Viau and C. Gatel, Phys. Rev. B, **80**, 064427 (2009)
[30] J. A. Osborn, Phys. Rev. **67**, 351 (1945)
[31] J. Jorzick, S. O. Demokritov, B. Hillebrands, M. Bailleul, C. Fermon, K. Y. Guslienko, A. N. Slavin, D. V. Berkov and N. L. Gorn, Phys. Rev. Lett. **88**, 047204 (2002)
[32] H. Fangohr, G. Bordignon, M. Franchin, A. Knittel, P. A. J. de Groot and T. Fischbacher, J. Appl. Phys. **105**, 07D529 (2009)
[33] R. Hertel, J. Appl. Phys. **90**, 5752 (2001)
[34] R. Hertel, J. Magn. Magn. Mater. **249,** 251 (2002)
[35] K. Nielsch, R. B. Wehrspohn, J. Barthel, J. Kirschner and U. Gösele Appl. Phys. Lett. **79**, 1360 (2001)
[36] J. De La Torre Medina, L. Piraux, J. M. Olais Govea and A. Encinas, Phys. Rev. B **81**, 144411 (2010)
[37] A. Encinas-Oropesa, M. Demand, L. Piraux, I. Huynen and U. Ebels, Phys. Rev. B **63**, 104415 (2001)